ARTICLE
Journal of Cellular Biochemistry 116:809–821 (2015)

Journal of Cellular Biochemistry

Transcriptome Analysis of Canine Cardiac Fat Pads: Involvement of Two Novel Long Non-Coding RNAs in Atrial Fibrillation Neural Remodeling

Weizong Wang,[1] Ximin Wang,[1] Yujiao Zhang,[1] Zhan Li,[1] Xinxing Xie,[1] Jiangrong Wang,[1] Mei Gao,[1] Shuyu Zhang,[2*] and Yinglong Hou[1**]

[1]*Department of Cardiology, Shandong Provincial Qianfoshan Hospital, Shandong University, Jinan 250014, China*

[2]*School of Radiation Medicine and Protection and Collaborative Innovation Center of Radiation Medicine of Jiangsu Higher Education Institutions, Soochow University, Suzhou 215123, China*

ABSTRACT

Intrinsic cardiac autonomic neural remodeling (ANR) has been reported to be involved in the initiation and maintenance of atrial fibrillation (AF). Long non-coding RNAs (lncRNAs) are important orchestrators of gene regulatory networks. However, little is known about the relationships between lncRNAs and cardiac ANR in AF. In this study, second-generation RNA sequencing was performed to examine the transcriptomes of lncRNAs in AF and non-AF canine cardiac fat pads. A total of 61,616 putative lncRNAs were yielded, in which 166 were downregulated and 410 were upregulated with more than twofold change. Bioinformatics analysis showed that the aberrantly expressed genes were associated with neural development, migration and neurodegenerative disorders. On the basis of a series of filtering pipelines, two new lncRNAs, namely, TCONS_00032546 and TCONS_00026102, were selected. Silencing of TCONS_00032546 or TCONS_00026102 with lentiviruses in vivo could significantly shorten or prolong the atrial effective refractory period thereby increasing or preventing AF inducibility by promoting or inhibiting the neurogenesis. Besides, the expression of CCND1-FGF19-FGF4-FGF3 gene cluster and SLC25A4, the nearby genes of TCONS_00032546 and TCONS_00026102, were negatively correlated with that of lncRNAs. Furthermore, combining bioinformatics analysis with literature review, TCONS_00032546 and TCONS_00026102 may induce effects by increasing the CCND1-FGF19-FGF3-FGF4 gene cluster and SLC25A4 via complex mechanisms during neural remodeling. Taken together, dysregulated lncRNAs may play regulatory roles in AF neural remodeling, which may further provide potential therapeutic targets for prophylaxis and treatment of AF. J. Cell. Biochem. 116: 809–821, 2015.

KEY WORDS: ATRIAL FIBRILLATION; AUTONOMIC NEURAL REMODELING; LONG NON-CODING RNA; TCONS_00032546; TCONS_00026102

Atrial fibrillation (AF) is the most common cardiac arrhythmia with complex mechanisms. In recent years, the role of the intrinsic cardiac autonomic nervous system in the pathogenesis of AF has drawn widespread attention. Autonomic innervation is inhomogeneous in the heart [Tan et al., 2006], which acts as an important factor in the initiation and perpetuation of AF. The occurrence of AF also exacerbates the uneven distribution of the autonomic nerves [Chang et al., 2001], causing nerve sprouting, that is, autonomic neural remodeling (ANR). Further studies indicated that ANR not only increases the onset of AF but also acts as an atrial substrate for the maintenance of AF [Otake et al., 2009; Ng et al., 2011], and autonomic denervation could abolish AF within a

Conflict of Interest: The authors declare that they have no competing interests.

This article has been accepted for publication and undergone full peer review but has not been through the copyediting, typesetting, pagination and proofreading process, which may lead to differences between this version and the Version of Record. Please cite this article as doi: [10.1002/jcb.25037].

Grant sponsor: National Natural Science Foundation of China; Grant numbers: 81270237, 81472920; Grant sponsor: Specialized Research Fund for the Doctoral Program of Higher Education of China; Grant number: 20110131110063; Grant sponsor: Foundation of Shandong Province; Grant number: ZR2012HM048; Grant sponsor: Priority Academic Program Development of Jiangsu Higher Education Institutions (PAPD).

*Correspondence to: Shuyu Zhang, School of Radiation Medicine and Protection, Soochow University, No. 199, Renai Road, Suzhou 215123, China. E-mail: zhang.shuyu@hotmail.com Correspondence to: Yinglong Hou, Department of Cardiology, Shandong Provincial Qianfoshan Hospital, No. 16766, Jingshi Road, Jinan, 250014, China. E-mail: houyinglong2010@hotmail.com

Manuscript Received: 24 April 2014; Manuscript Accepted: 11 December 2014

Accepted manuscript online in Wiley Online Library (wileyonlinelibrary.com): 5 January 2015

DOI 10.1002/jcb.25037 • © 2015 Wiley Periodicals, Inc.

relatively long period [Calò et al., 2012]. Therefore, ANR and AF are closely linked as cause-and-effect, which eventually develops into a vicious cycle. Stopping or even reversing the ANR may become a novel therapeutic approach for the treatment of AF. However, molecular mechanisms of cardiac ANR during AF remain elusive.

With the advancement of genome-wide sequencing and other related technologies, at least 90% of the mammalian genome is transcribed, but protein-coding genes represent only <2% of the total genome. The large proportion of the genome is transcribed into non-coding RNAs (ncRNAs) [Wu et al., 2010]. According to length, ncRNAs can be subdivided into small ncRNAs (shorter than 200 nucleotides) and long ncRNAs (lncRNAs), (longer than 200 nucleotides) [Yu et al., 2013]. Initially, lncRNAs are identified as transcriptional "noise" without biological functions [Shi et al., 2013]. However, evidence of conserved secondary structure and strict biological regulation suggest that lncRNAs possess biological functions [Mercer et al., 2009]. Subsequently, several lines of evidence have demonstrated that lncRNAs are involved in key biological processes including genomic imprinting, dosage compensation, chromatin remodeling, splicing regulation, and mRNA decay [Niland et al., 2012]. Currently, lncRNAs have been emerging as a new research hotspot in the pathogenesis of various diseases, including tumors [Wang et al., 2011], neuro-degenerative diseases [Clark and Blackshaw, 2014] and cardiovascular diseases [Ishii et al., 2006; Song et al., 2013; Zhu et al., 2014]. Moreover, lncRNAs have been shown to play indispensable roles in the development of central and peripheral nervous systems [Clark and Blackshaw, 2014; Yu et al., 2013].

Despite promising evidence that supports a close linkage between lncRNAs and cardiac ANR in AF, little is known about the relationship between lncRNAs and AF neural remodeling. Given that cardiac fat pads serve as distribution and integration centers of the intrinsic cardiac autonomic nerves [Hou et al., 2007], which are the most intensive and obvious areas of neural remodeling in the atrium [Armour et al., 1997], next-generation RNA sequencing (RNA-Seq) was performed in the anterior right fat pads (ARFPs) to compare the expression patterns of lncRNAs between AF and non-AF canines. Filtering methods were also used to select AF-related lncRNAs. Furthermore, the potential involvement of the identified lncRNAs in AF neural remodeling was investigated in this study.

MATERIALS AND METHODS

ANIMAL PREPARATION

Six adult beagle dogs weighing 20–30 kg of either sex were randomly divided into two groups: AF (n = 3) and control (n = 3). The AF group underwent continuous atrial tachypacing (400 beats/min) for 4 weeks. The dogs were anesthetized with 30 mg/kg of intravenous Na-pentobarbital and ventilated with room air by a positive-pressure respirator. Four electrode endocardial leads attached to pacemakers (AOO, made in Fudan University, China) were inserted into the right atrial appendage through jugular veins. The pacemakers were implanted in subcutaneous pockets to achieve permanent pacing. The control group was sham-operated in the same way as the AF group but without pacing. Standard electrocardiogram (ECG) lead II and blood pressure were continuously monitored on the Electrophysiology Management System of LEAD-7000 (Sichuan Jinjiang Electronic Science and Technology Co., Ltd., Sichuan, China). Surface ECGs were recorded every week to examine the occurrence of AF by turning off the pacemakers. The dog developed AF if a period of rapid irregular atrial rhythm lasted for at least 30 s. The study was performed in accordance with the Guidelines for the Care and Use of Laboratory Animals published by the National Institutes of Health (NIH publication no. 85–23, revised 1996). The experimental protocol was approved by the Ethics Committee of Shandong University.

TISSUE PROCESSING

After 4 weeks of continuous pacing, all animals were sacrificed by air embolism. ARFPs, including underlying muscles, were obtained from all animals. Portions of the tissues were fixed in 4% formaldehyde for at least 48 h, dehydrated, embedded in wax, and sectioned into 3 μm thicknesses. The remaining samples were stored at −80°C until use.

IMMUMOHISTOCHEMISTRY ANALYSIS

Briefly, anti-protein gene product 9.5 (PGP9.5) antibodies (Abcam, Cambridge, UK; used at 1:30) were used for immunocytochemical staining. Details of the staining techniques have been published elsewhere [Zheng et al., 2014]. Nerve density was determined using a computer-assisted image analysis system (Image-Pro Plus 6.0, Media Cybernetics, Inc., Rockville, MD). To eliminate artificial errors, the nerve density was quantified by a blind investigator. Each slide was examined at 20 × magnification under a microscope (Olympus, Tokyo, Japan). Three fields with the highest nerve densities were selected. The mean nerve density was calculated as the average density of the slices.

HIGH-THROUGHPUT RNA-SEQ

Total RNA was isolated from each sample by using TRIzol reagent (Invitrogen, Carlsbad, CA) according to the manufacturer's protocol. Equivalent RNAs from three samples in each group were mixed into a total sample for RNA-Seq. The RNA concentration of each sample was determined by measuring the absorption at 260 and 280 nm using a K5600 micro-spectrophotometer (Beijing Kaiao Technology Development Co., Ltd., Beijing, China).

High-throughput RNA-Seq of the two mixed samples was performed on Illumina Hiseq2500 with a 50 bp single-end protocol (Illumina, Inc., San Diego, CA). Given that the poor-quality fractions of the sequencing data were highly distributed in the end, Trim Galore software was used to dynamically remove the poor-quality segments and to connect the sequence segments. Then, FastQC (http://www.bioinformatics.babraham.ac.uk//projects/fastqc/) software was adopted for quality control analysis. Subsequently, TopHat (http://tophat.cbcb.umd.edu/) was used to map the pre-proposed reads to *Canis* reference (ftp://igenome:G3nom3s4u@ussd-ftp.illumina.com/Canis_familiaris/Ensembl/BROADD2/Canis_familiaris_Ensembl_BROADD2.tar.gz) and analyze the mapping results to identify splice junctions between the exons. The mapping reads were arranged using Cufflinks (http://cufflinks.cbcb.umd.edu/) to assemble transcripts and estimate their abundance [Trapnell et al., 2010]. The annotated locations of the transcripts were also compared with that of the known reference using Cuffcompare software. The comparative results indicated that unknown intergenic transcripts,

potentially novel isoforms, intron transcripts, multiple-exon transcripts, and antisense transcripts overlapping within reference exons and introns were characterized as preliminary candidate lncRNAs. Candidate lncRNAs were acquired by satisfying the following criteria: RNA length ≥ 200 nt, CPC score ≤ 0, CPAT probability ≤ 0.364, and phyloCSF score ≤ -20. The raw sequencing data have been submitted to the NCBI and are accessible at http://www.ncbi.nlm.nih.gov/sra/?term = SRX393125.

The expression levels of the transcripts were calculated by fragments per kilobase of transcript per million fragments mapped (FPKM) values. Differentially expressed transcripts (DETs) were defined as $P < 0.05$ and/or fold change >2 times based on their FPKM values between the groups, which were identified using Cuffdiff software.

QUANTITATIVE REAL-TIME PCR

Reverse-transcribed cDNA was synthesized by 1 μg of total RNA using RevertAid First Strand cDNA Synthesis Kit (Thermo Scientific, Vilnius, Lithuania). Quantitative real-time PCR (qRT-PCR) analysis was conducted with Maxima SYBR Green/ROX qPCR Master Mix (2X) (Thermo Scientific) on the ABI ViiA 7 Real-Time PCR system (Applied Biosystems, Foster City, CA). Each sample was tested in triplicate. The relative gene expression levels were calculated using $2^{-\Delta\Delta Ct}$ method against *GAPDH* for normalization. The gene-specific primers used for amplification are listed in Supplemental Table SI.

GO AND KEGG PATHWAY ANALYSIS

Gene ontology (GO) was adopted to annotate the functions of differentially expressed genes in the GO vocabularies. Briefly, the differentially expressed genes were regarded as candidates from the whole genes. The enrichment *P*-value was confirmed between the GO feature sets and the differentially expressed genes were calculated using a hypergeometric distribution test. The *P*-value was further corrected by Benjamini–Hochberg multiple test to obtain the false discovery rate (FDR). Based on *P*-value and FDR, the enrichment score was expressed in −log 10(*P*-value). Kyoto Encyclopedia of Genes and Genomes (KEGG) pathway analysis was also applied to define the functions of the differentially expressed genes in graphical diagrams of biochemical pathways. KEGG pathway analysis was similar to that of GO functional analysis. The significance was calculated by FDR and *P*-value.

TARGET GENE PREDICTION

Cis- and *trans*-predictions were used to identify the target genes of the differentially expressed lncRNAs. For *cis*-prediction, a systematic search was performed based on the genomic location of the lncRNAs to identify the known protein-coding transcripts. Interactions between the known protein-coding transcripts and the differentially expressed lncRNAs can be divided into three categories: (i) antisense transcripts—the known protein-coding transcripts were overlapped with the lncRNAs, and the transcriptional orientation of the known protein-coding transcripts was opposite to that of the lncRNAs; (ii) fragments of mRNA sequence—the exons or introns of the known protein-coding transcripts were overlapped with the lncRNAs and both transcripts shared the same transcriptional orientation; and (iii) transcripts from promoter regions—the 3 kb upstream or downstream sequences from transcriptional start sites of the known protein-coding transcripts were overlapped with the lncRNAs.

For *trans*-prediction, Basic Local Alignment Search Tool (BLAST) sequence comparison between the lncRNAs and 3′UTR of the known protein-coding transcripts was performed to assess the possibility of forming complexes. The criteria of the BLAST sequence analysis indicated that the ratio between the target and query sequence lengths should be $>10\%$.

CONSTRUCTION OF LENTIVIRUSES

Scrambled shRNA (negative control) and four shRNAs targeting TCONS_00032546 or TCONS_00026102 were designed by GenePharma (Shanghai GenePharma Co., Ltd., Shanghai, China). The shRNA sequences are listed in Supplemental Table SII. To produce the lentiviruses, a shuttle vector containing shRNA fragments and packaging plasmids consisting of pGag/Pol, pRev, and pVSV-G were co-transfected into 293T cells by RNAi-Mate (GenePharma). The viral particles were harvested at 72 h post-transfection. After purification and concentration, the recombinant lentiviral vectors were obtained with a titer of 1×10^9 TU/ mL for injection.

INFECTION OF LENTIVIRUSES

Fifteen adult beagle dogs of either sex were randomly allocated into three groups: (i) control (n = 5), infected with control lentivirus; (ii) lenti-RNAi-TCONS_00032546 (n = 5), infected with lentiviruses targeting TCONS_00032546; and (iii) lenti-RNAi-TCONS_00026102 (n = 5), infected with lentiviruses targeting TCONS_00026102. Right thoracotomy was performed at the fourth intercostal space, and the hearts were exposed after excising the pericardium. Up to 100 μL of the mixed lentiviruses consisting of two *Lentivirus* species were directly injected into 10 separate sites in ARFP to achieve even distribution. The chest was then closed, and air in the thoracic cavities was evacuated. Samples were collected 10 d after infection. Some of the samples were used for immunohistochemical staining and others were stored at −80°C until use.

ELECTROPHYSIOLOGICAL MEASUREMENTS

Atrial effective refractory period (AERP) and AF inducibility were determined after thoracotomy (before infection), immediately after infection and 10 d after infection. Programmed electrical stimulation (PES) (LEAD-7000) was used by placing a catheter in the right atrium located <0.5 cm around the ARFP. The AERP was defined as the longest S1–S2 interval failing a propagated response. Briefly, following a 30 s conditioning stimulation period at basic cycle lengths of 200 ms, the S1–S2 intervals started at 150 ms, followed by decrements of 5 ms (S1: S2 = 8: 1) until no more atrial response was propagated. AF was induced by PES with burst stimulation twice the diastolic threshold (cycle length of 120 ms, lasting 2–3 min). Rapid irregular atrial rhythms lasting >30 s were regarded as successful inductions of AF. The procedure was repeated thrice for each measurement.

MECHANISM PREDICTION OF LNCRNAS

For prediction of lncRNA mechanisms, the methods demonstrated by Guttman et al. [2009] were adopted. For specific lncRNAs, the co-expressed mRNAs were generally ranked by calculating Pearson correlation. The top-100 ranked mRNAs were identified based on

Pearson correlation with P-value < 0.05. A functional enrichment analysis was conducted in this set of co-expressed mRNAs using hypergeometric cumulative distribution function. The enriched functional terms were categorized and determined as the predicted mechanisms of the given lncRNA.

STATISTICAL ANALYSIS

Statistical analysis was performed using SPSS 17.0 software (IBM Corp., Armonk, NY). All data were expressed as mean ± standard error of mean. For sequencing data, paired-sample t-test was used to compare the expression of lncRNAs. For qRT-PCR data, unpaired t-test was used to compare the gene expression levels between the groups. All P-values were two-sided, and $P < 0.05$ was considered statistically significant.

RESULTS

ANR IS ACCOMPANIED BY OCCURRENCE OF AF

AF models were successfully established in all canines receiving right atrial tachypacing. Examples of the sinus rhythm and the AF surface ECGs are shown in Supplemental Figure S1A and B. The extent of ANR was examined via immunohistochemical staining and nerve density determination. Compared with the control group, the number of the PGP-9.5-positive neurons significantly increased in the AF group, and the newborn neurons in the fat pads were more numerous and larger (Supplemental Fig. S1C and D). Correspondingly, the nerve density increased in the AF group with statistical significance (4.98 ± 0.78 vs. $13.9 \pm 3.51 \times 10^5$ $\mu m^2/mm^2$, $P = 0.0015$).

ALIGNMENT OF SEQUENCING READS

Using the Illumina Hiseq2500 platform, the total raw reads ranged from 35 million to 40 million, and the average quality score was 36. TopHat aligner indicated that about 29–33 million reads were uniquely mapped to the canine genome sequence (Supplemental Table SIII). No obvious differences regarding the percentage of genomic alignment (AF vs. control: 83.13% vs. 83.61%), and the density distributions of the reference genome among chromosomes were observed, suggesting slight bias in the sequencing results. Repetition of reads was evaluated by two strategies: one was based on identical read sequences and the other was comparable to the corresponding genome location (Supplemental Fig. S2A). The distribution of the total mapped reads onto the genome showed that 67.74% were aligned at the exons and UTR regions, 15.53% at the introns, and others within the 10 kb upstream and downstream of the transcripts (Supplemental Fig. S2B). Uniform distributions of the transcripts elucidated that the quality of the RNA-Seq was excellent, which was verified by data analysis.

ANALYSIS OF DIFFERENTIALLY EXPRESSED LNCRNAS

A total of 61,616 putative lncRNAs were yielded, in which 2593 transcripts contained multiple exons. Then 116 transcripts were eliminated because of transcript length ≤ 200 nt. After filtering based on CPC score, CPAT probability, and phyloCSF score, 1164 transcripts were reserved as candidate lncRNAs. Based on FPKM values, 576 DETs exhibited more than twofold change and $P < 0.05$, in which 166 transcripts were downregulated and 410 were upregulated [Wang and Hou, 2014]. In the aberrantly expressed transcripts, 45 were identified as new DETs [Wang and Hou, 2014]. Among these DETs, 15 were upregulated and 30 were downregulated. A volcano plot elucidated the variance in DETs based on P-value and fold change (Supplemental Fig. S2C). The new lncRNAs were further displayed by heat map (Fig. 1). Correspondingly, the fold changes of the new DETs are listed in Table I.

QUANTIFICATION OF LNCRNA EXPRESSION

To validate the RNA-Seq results, three upregulated and three downregulated lncRNAs were randomly selected from the new DETs. The relative expression levels of these new DETs were analyzed by qRT-PCR in the six samples. The expression trends were consistent with those obtained from the RNA-Seq. Specifically, the expression of the upregulated TCONS_00113767, TCONS_00017223, and TCONS_00008295 and the downregulated TCONS_0023347 reached statistical significance, which was consistent with the RNA-Seq results. However, TCONS_00008479 and TCONS_00011580 expression showed no difference between the groups, which failed to match with the RNA-Seq results (Fig. 2A).

GO AND KEGG PATHWAY ANALYSES

Differentially expressed genes were categorized and annotated by GO functional analysis, which used three structured and controlled vocabularies to describe the gene products in terms of associated biological processes, cellular components and molecular functions. The results showed that the functions of the aberrantly expressed genes mainly involved the following biological processes: (i) GO:2000026 regulation of multicellular organismal development; (ii) GO:0051094 positive regulation of developmental process; (iii) GO:0023051 regulation of signaling; (iv) GO:0072358 cardiovascular system development; (v) GO:0016477 cell migration; and (vi) GO:0045161 neuronal ion channel clustering (Supplemental Fig. S3A).

The KEGG pathway consists of a number of graphical diagrams illustrating the molecular interactions and reaction networks. The KEGG pathway analysis indicated that the differentially expressed genes were enriched in the following pathways: (i) cfa03015 mRNA surveillance pathway; (ii) cfa05414 dilated cardiomyopathy; (iii) cfa04540 gap junction; (iv) cfa00564 glycerophospholipid metabolism; (v) cfa04020 calcium signaling pathway; and (vi) cfa05012 Parkinson′s disease (Supplemental Fig. S3B).

IDENTIFICATION OF CANDIDATE LNCRNAS

The identification process of candidate lncRNAs in AF neural remodeling is described as follows. First, lncRNAs with more than an absolute twofold change were selected. Subsequently, according to the functions of the predicted target genes, DETs by which the target genes were associated with nerve growth, nerve development, nerve migration, and neurological diseases were selected. Aiming at the identified target genes, GO and KEGG pathway analyses were also conducted. With these three steps, one upregulated and two downregulated lncRNAs were selected. Finally, considering that lncRNAs were tissue-specific, the expression of the three selected lncRNAs was examined by qRT-PCR in six canine skeletal muscles to exclude muscle-derived lncRNAs (Fig. 2B). The results showed that

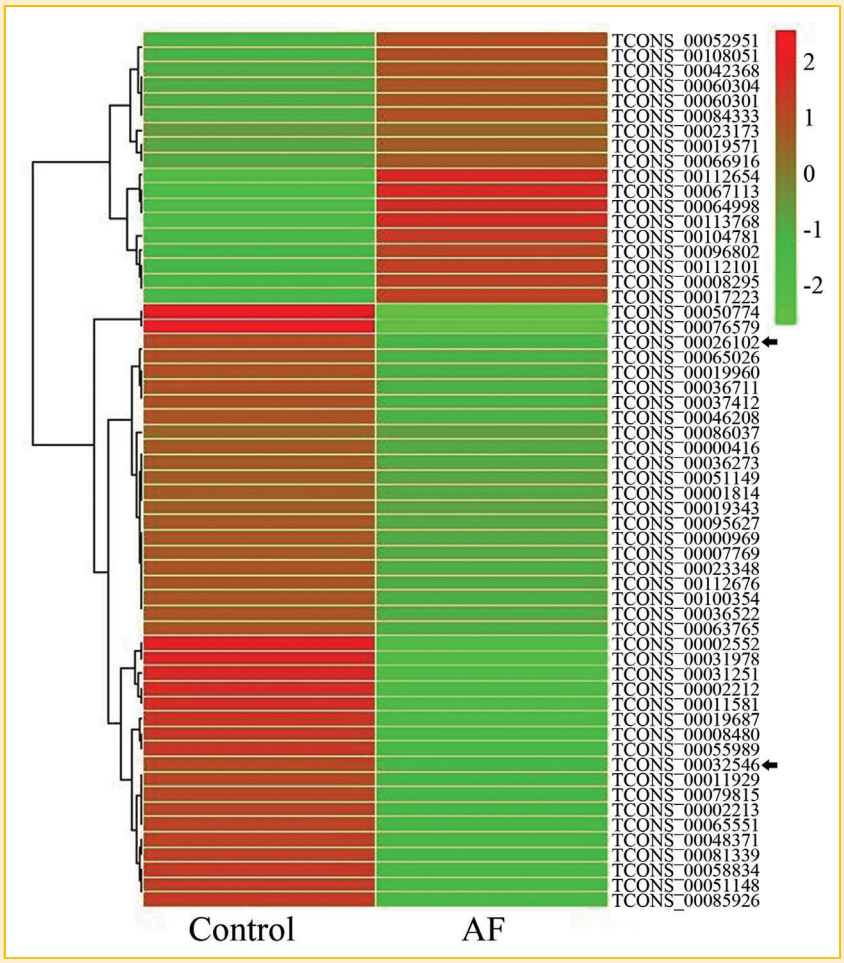

Fig. 1. Heat map of the new lncRNAs between the two groups. Expression levels are reflected by color change. Red denotes higher expression, whereas green denotes lower expression. TCONS_00032546 and TCONS_00026102 are marked with black arrows.

TCONS_00032546 and TCONS_00026102 can be used for further analysis.

OVERVIEW OF TCONS_00032546 AND TCONS_00026102

On the based of sequence similarity, the mechanisms between lncRNAs and their target genes were classified into three forms [Bu et al., 2012]: 3′UTR, 3 kb upstream or downstream and antisense. According to the three mechanisms, 445 aberrantly expressed lncRNAs were eligible to predict the target genes, in which 11 transcripts were new DETs (Table II). Both TCONS_00032546 and TCONS_00026102 were downregulated new lncRNAs. Sequence analysis using the Ensemble BLAST revealed that TCONS_00032546 was located on the reverse strand of chromosome 18:48471639–48473748 (Canfam 3.1), and the transcript belongs to long intergenic ncRNAs (lincRNAs), which do not intersect with any protein-coding loci [Clark and Blackshaw, 2014]; TCONS_00026102 was located on the reverse strand of chromosome 16:45460536–45470026 (Canfam 3.1), and the transcript is also categorized as lincRNA. The predicted target genes of TCONS_00032546 and TCONS_00026102 were fibroblast growth factor 19 (FGF19) and solute carrier family 25 member 4 (SLC25A4), respectively. Bioinformatics analysis showed that TCONS_00032546/TCONS_00026102 were transcribed from the 3 kb upstream or downstream of the transcriptional start site of FGF19/SLC25A4. GO analysis showed that FGF19 was involved in neural crest cell migration (GO:0001755), development (GO:0014032), and differentiation (GO:0014033). Pathway analysis indicated that SLC25A4 was associated with Parkinson′s disease (cfa05012). TCONS_00032546 was positively correlated with FGF19, whereas TCONS_00026102 was negatively correlated with its target gene as validated by qRT-PCR (Fig. 2C).

BIOLOGICAL EFFECTS OF TCONS_00032546 AND TCONS_00026102 IN AF

Lentiviruses against TCONS_00032546 and TCONS_00026102 were constructed and transfected into the ARFPs to further investigate whether the two transcripts affected AF neural remodeling. To improve knockdown efficiency, the ARFPs were co-infected with two specific lentiviruses, which acted at the same lncRNA. After 10 d infection, qRT-PCR analyses revealed that both TCONS_00032546 and TCONS_00026102 targeting lentiviruses could remarkably reduce the expression of their corresponding lncRNAs compared with that of

TABLE I. Fold Changes of the New DETs in Canine Models of AF

lncRNA transcript id	Fold change	*P*-value	lncRNA transcript id	Fold change	*P*-value
TCONS_00052951	2.228	0.00295	TCONS_00051149	−1.678	0.0165
TCONS_00108051	2.739	0.00005	TCONS_00001814	−1.978	0.03
TCONS_00042368	2.202	0.03845	TCONS_00019343	−2.333	0.0043
TCONS_00060304	2.138	0.0349	TCONS_00095627	−2.284	0.0112
TCONS_00060301	1.983	0.0203	TCONS_00000969	−1.552	0.0236
TCONS_00084333	2.322	0.01985	TCONS_00007769	−10.434	0.02245
TCONS_00023173	0.976	0.0013	TCONS_00023348	−11.405	0.0382
TCONS_00019571	1.74	0.0477	TCONS_00112676	−1.636	0.03325
TCONS_00066916	2.69	0.0447	TCONS_00100354	−2.011	0.03525
TCONS_00112654	3.986	0.00005	TCONS_00036522	−1.901	0.0299
TCONS_00067113	8.651	0.00245	TCONS_00063765	−1.902	0.04405
TCONS_00064998	4.181	0.0299	TCONS_00002552	−15.519	0.03025
TCONS_00113768	3.462	0.0007	TCONS_00031978	−3.821	0.00005
TCONS_00104781	5.273	0.0012	TCONS_00031251	−9.456	0.0035
TCONS_00096802	3.769	0.0012	TCONS_00002212	−3.459	0.0488
TCONS_00112101	4.291	0.00245	TCONS_00011581	−12.297	0.02655
TCONS_00008295	2.982	0.03625	TCONS_00019687	−4.371	0.0082
TCONS_00017223	2.816	0.01285	TCONS_00008480	−12.361	0.00405
TCONS_00050774	−25.338	0.0011	TCONS_00055989	−10.63	0.00725
TCONS_00076579	−23.737	0.00155	**TCONS_00032546**	**−2.349**	**0.00305**
TCONS_00026102	**−2.237**	**0.04095**	TCONS_00011929	−3.481	0.002
TCONS_00065026	−2.344	0.02855	TCONS_00079815	−2.578	0.0209
TCONS_00019960	−2.426	0.00155	TCONS_00002213	−3.087	0.01335
TCONS_00036711	−2.131	0.0353	TCONS_00065551	−3.564	0.0245
TCONS_00037412	−1.975	0.01115	TCONS_00048371	−4.331	0.0011
TCONS_00046208	−1.828	0.01395	TCONS_00081339	−3.409	0.03
TCONS_00086037	−1.659	0.04125	TCONS_00058834	−12.539	0.00935
TCONS_00000416	−2.183	0.01675	TCONS_00051148	−4.9	0.00035
TCONS_00036273	−1.722	0.02545	TCONS_00085926	−14.315	0.04095

TCONS_00032546 and TCONS_00026102 are highlighted in bold.

the negative control (Fig. 4A). Subsequently, electrophysiological parameters of the experimental and control groups were compared to examine their biological roles in AF initiation. The AERP in the ARFPs did not reach statistical significance before and immediately after infection (Fig. 4B). However, after 10 d infection, TCONS_00032546 knockdown could significantly shorten the AERP (100.56 ± 1.94 vs. 110.56 ± 1.30, $P = 0.0085$), while repressing TCONS_00026102 expression significantly prolonged the AERP (131.11 ± 1.62 vs. 110.56 ± 1.30, $P < 0.0001$) (Fig. 4B). Compared with the control group in which paroxysmal atrial tachycardia (lasting <30 s) was induced in two dogs, AF was induced in two out of five animals, and paroxysmal atrial tachycardia existed in all five animals in the lenti-RNAi-TCONS_00032546 group. By contrast, no paroxysmal atrial tachycardia and AF induction were observed in the lenti-RNAi-TCONS_00026102 group. Despite lack of significant difference, these findings suggested that the downregulation of TCONS_00032546 could increase the inducibility of AF. However, decreasing the expression of TCONS_00026102 showed an opposite effect.

To further validate whether the influence of the two lncRNAs on AF initiation was related to neural remodeling, protein and mRNA levels of PGP9.5, which is a sensitive neuron-specific marker [Ootsuka et al., 2008], were measured. The results of immunohistochemical staining of PGP9.5 indicated that the neurons were more numerous and intensive in the lenti-RNAi-TCONS_00032546 group (Fig. 3B) than in the control group (Fig. 3A). However, these results were opposite to those in the lenti-RNAi-TCONS_00026102 group (Fig. 3C). Correspondingly, the nerve density in the lenti-RNAi-TCONS_00032546 group was significantly higher than that in the control group (14.80 ± 1.37 vs. $4.95 \pm 0.81 \times 10^5\ \mu m^2/mm^2$, $P = 0.0032$, Fig. 3D). By contrast, silencing of TCONS_00026102 decreased the nerve density (0.35 ± 0.59 vs. $4.95 \pm 0.81 \times 10^5\ \mu m^2/mm^2$, $P = 0.0001$, Fig. 3D). Subsequently, growth-associated protein 43 (GAP43) and PGP9.5 were examined by qRT-PCR to validate the immunohistochemical staining results. The results of GAP43, which plays a key role in neurite formation, regeneration, and plasticity [Spencer et al., 1992], agreed with those of immunohistochemical staining (Fig. 4C). However, the mRNA expression levels of PGP9.5 were not entirely consistent with the changes of its protein levels (Fig. 4C). Compared with the control group, the PGP9.5 mRNA level significantly increased in the lenti-RNAi-TCONS_00032546 group. However, no significant difference existed between the lenti-RNAi-TCONS_00026102 and control groups, suggesting that the expression of PGP9.5 may be regulated post-transcriptionally.

POTENTIAL MECHANISMS OF TCONS_00032546 AND TCONS_00026102 IN AF NEURAL REMODELING

To explore the potential mechanisms by which the two lncRNAs affected AF neural remodeling, the expression levels of the target genes belonging to the two lncRNAs were initially assessed by qRT-PCR. Both FGF19 and SCL25A4 significantly increased in the

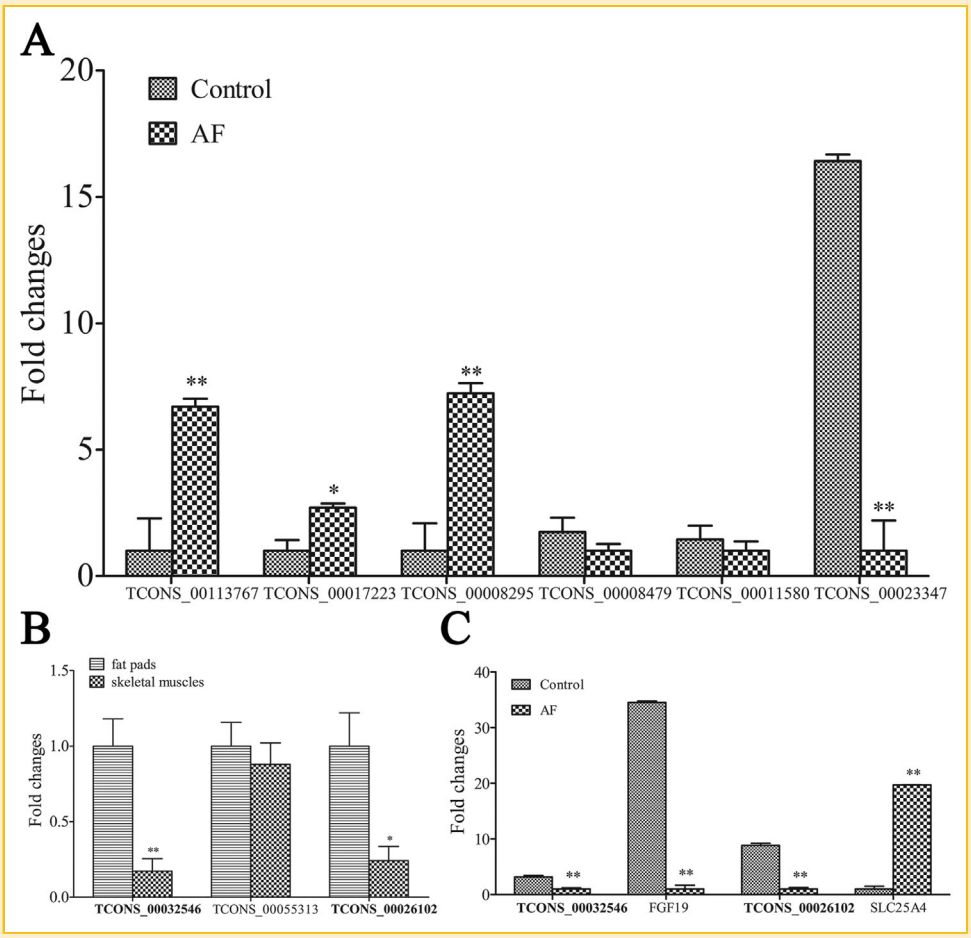

Fig. 2. Identification of candidate lncRNAs in AF neural remodeling. (A) Expression levels of six differentially expressed new lncRNAs were confirmed in three paired AF/non-AF intracardiac fat pads. (B) Expression levels of three candidate lncRNAs were compared in fat pads and skeletal muscles. (C) Expression levels of two candidate lncRNAs and their associated target genes were compared in three paired AF/ non-AF intracardiac fat pads. TCONS_00032546 and TCONS_00026102 are highlighted in bold. $^{*}P < 0.05$ and $^{**}P < 0.01$.

experimental groups (Fig. 4D and E). In addition, lincRNAs could regulate the expression of the neighboring genes residing within 300 kb of their locus [Ponjavic et al., 2009]. Thus, the expression levels of nearby protein-coding genes were also examined. The expression levels of FGF3, FGF4 and cyclin D1 (CCND1) increased 7.4, 3.3, and 4.9-fold, respectively, in the lenti-RNAi-TCONS_00032546 group (Fig. 4D). However, no other differentially expressed gene was detected in the lenti-RNAi-TCONS_00026102 group (Fig. 4E). Both bioinformatics analysis and literature review demonstrated that FGF3, FGF4, and FGF19 were clustered in canine chromosome 18 near the

TABLE II. Results of the Predicted Target Genes in New DETs

lncRNA transcript id	Target gene id	Target gene name	Possible mechanism	Target gene fold change
TCONS_00112101	ENSCAFG00000010945	PPP2R3B	upstream 3 kb or downstream 3 kb	−1.111
TCONS_00032546	**ENSCAFG00000010693**	**FGF19**	**upstream 3 kb or downstream 3kb**	**−12.563**
TCONS_00031251	ENSCAFG00000010557	GTPBP8	3′UTR	1.33
TCONS_00055989	ENSCAFG00000012386	KLHL30	antisense	1.627
TCONS_00079815	ENSCAFG00000009748	SYCP2L	antisense	−1.168
TCONS_00007769	ENSCAFG00000007340	PDHB	upstream 3 kb or downstream 3 kb	−1.312
TCONS_00000969	ENSCAFG00000002572	SBK2	upstream 3 kb or downstream 3 kb	−1.986
TCONS_00023348	ENSCAFG00000007476	HCFC2	upstream 3 kb or downstream 3 kb	−0.066
TCONS_00026102	**ENSCAFG00000007596**	**SLC25A4**	**upstream 3 kb or downstream 3kb**	**1.507**
TCONS_00063765	ENSCAFG00000011219	ADRB1	upstream 3 kb or downstream 3 kb	−1
TCONS_00019571	ENSCAFG00000008589	ART3	3′UTR	−0.24

TCONS_00032546 and TCONS_00026102 are highlighted in bold.

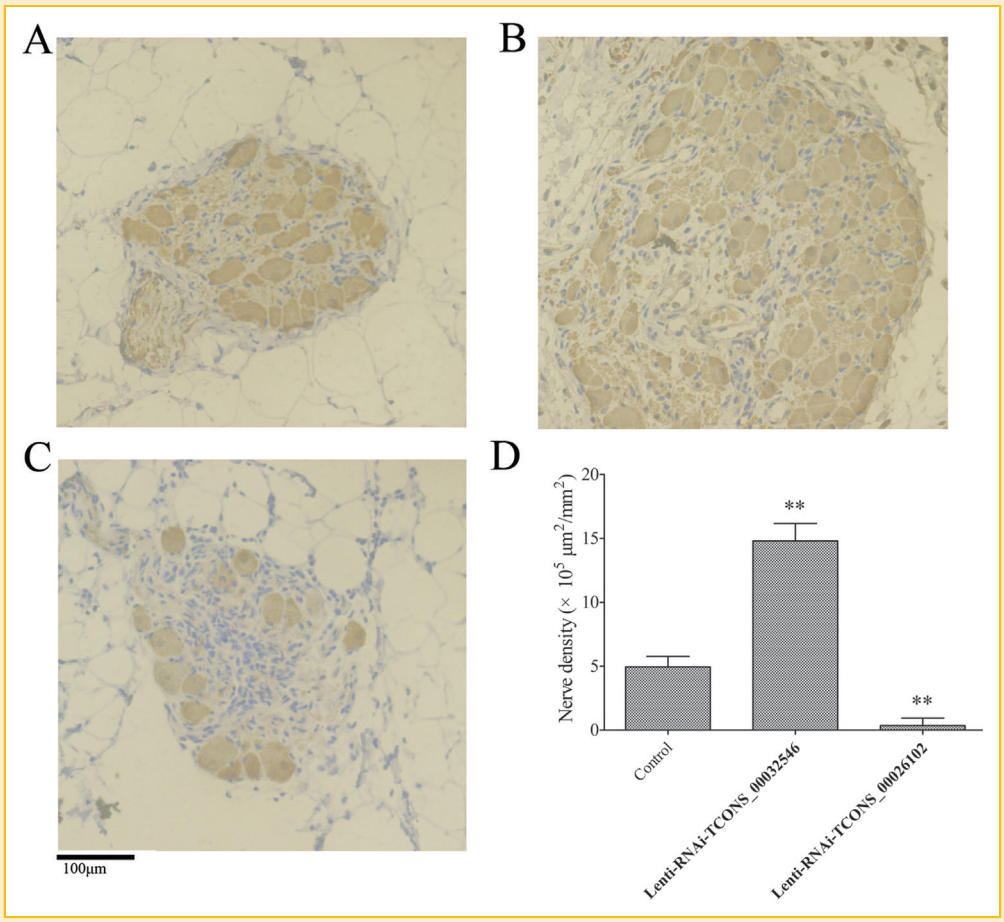

Fig. 3. Measurement of nerve density by immunohistochemical analysis. (A–C) Immunohistochemical staining of PGP9.5-positive neurons within ARFPs in the control (A), lenti-RNAi-TCONS_00032546 (B), and lenti-RNAi-TCONS_00026102 (C) groups. (D) Histograms of mean PGP9.5-positive nerve density in ARFPs. The brown granules represent PGP-9.5-positive neurons. Magnification, 20 ×. TCONS_00032546 and TCONS_00026102 are highlighted in bold. $^{**}P < 0.01$ compared with the control samples.

CCND1 gene, and the CCND1-FGF19-FGF4-FGF3 gene cluster was implicated in embryogenesis and carcinogenesis [Salmon et al., 2007]. Therefore, the CCND1-FGF19-FGF4-FGF3 gene cluster was a potential target of TCONS_00032546. Many studies demonstrated that the lincRNAs could also act in trans [Clark and Blackshaw, 2014]. Therefore, based on Pearson correlation and *P*-value, a set of co-expressed mRNAs of the two transcripts was identified and further used to predict the mechanisms of the two lincRNAs through GO and KEGG pathway analyses. The top five ranked GO and KEGG pathway terms are listed in Figure 5. Increasing studies suggested that MAPK pathway, which is tightly linked with the positive regulation of ERK1 and ERK2 cascade, plays an important role in mediating CCND1, FGF19, FGF4, and FGF3 in neurogenesis [Tamimi et al., 2006; Chen et al., 2010; Weisinger et al., 2010; Duan et al., 2013]. Meanwhile, overexpression of SLC25A4 could induce apoptosis, which is required for recruiting of NF-kappa B [Zamora et al., 2004]. The involvement of NF-kappa B pathway in the development of the nervous system, ranging from neuronal survival to synaptogenesis and plasticity, is also widely documented [Crampton and O'Keeffe, 2013]. Therefore, based on functional terms and literature search, the results exhibited that the CCND1-FGF19-FGF4-FGF3 gene cluster and SLC25A4 were strongly coupled with MAPK and NF-kappa B pathway, respectively. Compared with the control group, the qRT-PCR results showed that increased levels of ERK1/2, JNK, and p38 were observed in the lenti-RNAi-TCONS_00032546 group (Fig. 4F). And the nerve density decreased in the lenti-RNAi-TCONS_00026102 group, indicating that TCONS_00026102 knockdown could promote neural apoptosis in the intrinsic cardiac nervous system. Given these findings, we predicted that the biological effects of TCONS_00032546 may be attributed to an elevation in CCND1-FGF19-FGF4-FGF3 gene cluster through activation of the MAPK pathway, while TCONS_00026102-induced neural remodeling may be partially attributed to an increased expression level of SLC25A4 through the NF-kappa B pathway.

DISCUSSION

Recent high-throughput technologies have revealed that the transcriptomes of lncRNAs are involved in a variety of cardiac diseases, including ventricular septal defects [Song et al., 2013], myocardial

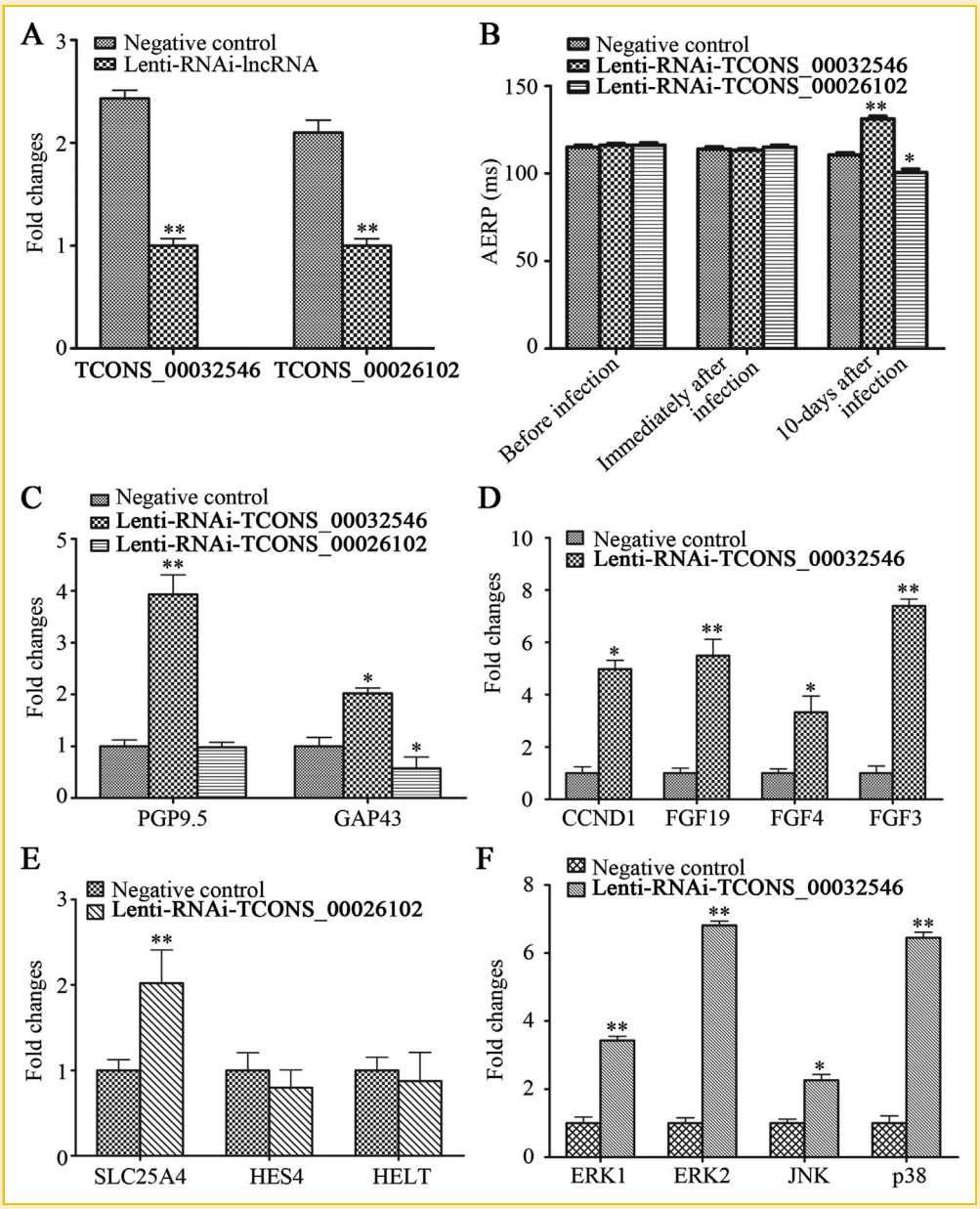

Fig. 4. Functions and predicted mechanisms of TCONS_00032546 and TCONS_00026102. (A) Expression levels of TCONS_00032546 and TCONS_00026102 were examined in ARFPs 10 d post-infection. (B) AERP was measured at three time points in ARFPs. (C) mRNA levels of PGP9.5 and GAP43 were compared in three groups after 10 d infection. (D, E) Expression levels of nearby protein-coding genes of TCONS_00032546 (D) and TCONS_00026102 (E) were compared between the control and experimental groups after 10 d infection. (F) Expression levels of ERK1/2, JNK, and p38 were assessed between the control and lenti-RNAi-TCONS_00032546 groups. TCONS_00032546 and TCONS_00026102 are highlighted in bold. *$P < 0.05$ and **$P < 0.01$.

infarction [Ishii et al., 2006], heart failure [Zhu et al., 2014] and so on. However, the expression patterns of lncRNAs and their potential involvement in AF neural remodeling have not been reported. In this study, the lncRNA expression profiles were investigated in AF and non-AF canine cardiac fat pads by using RNA-Seq technique. Several lncRNAs aberrantly expressed in AF neural remodeling were found and further characterized by annotating their dysregulated genes. The candidate lncRNAs, TCONS_00032546 and TCONS_00026102, were also selected, and their functions in the AF neural remodeling were identified. Moreover, predicted mechanisms about the novel lncRNAs were discovered. Thus, our findings provided not only transcriptome analysis of lncRNAs but also the biological effects of the two novel lncRNAs in AF neural remodeling, which may facilitate further studies.

Compared with microarrays, RNA-Seq is more sensitive in identifying potentially novel transcripts, as well as in detecting

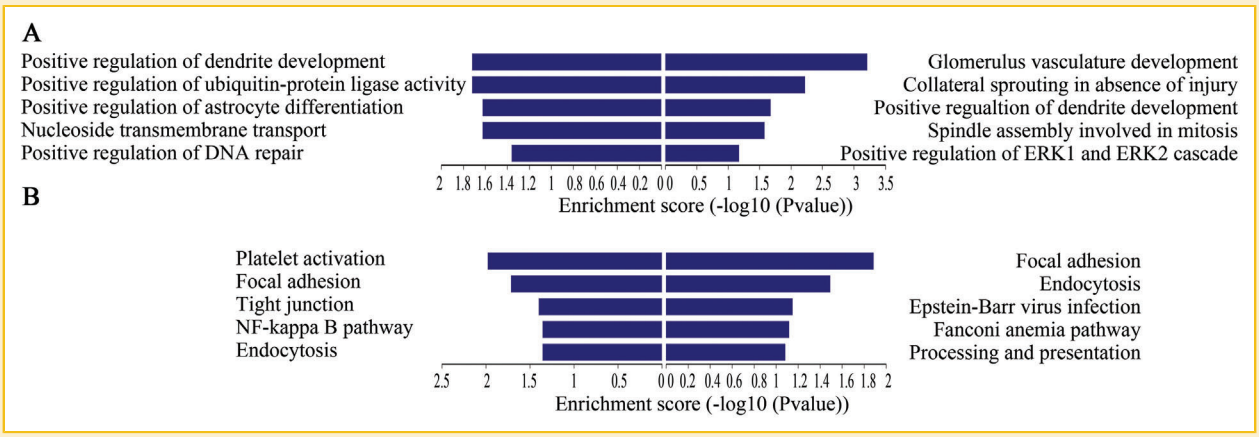

Fig. 5. Enriched functional terms of TCONS_00032546 (right) and TCONS_00026102 (left). The first five GO ID (A) and pathways (B) with the lowest *P*-value showed the biological processes that the two lncRNAs may be involved in.

low expressed genes, splice variants, and single-nucleotide polymorphisms [Merrick et al., 2013]. Besides, due to the limited transciptome information of lncRNAs in canine models, predefined probes for hybridization are currently insufficient. Therefore, RNA-Seq may provide more accurate and comprehensive information, particularly for the identification of novel molecules. Canines are usually regarded as valuable models for studying the pathogenesis of cardiac diseases, specifically AF. To our knowledge, this study is the first to investigate the lncRNA profiles during AF neural remodeling in canine models using RNA-Seq, which is helpful for better understanding the expression changes of lncRNAs in canine pathological conditions. Although lncRNAs are widely distributed within mammalian genomes, these transcripts are less conserved across species [Clark and Blackshaw, 2014]. To clarify the potential functions and mechanisms of lncRNAs in ANR, the transcriptome of lncRNAs should be characterized, and their potential involvement in cardiac fat pads during AF must be identified.

To eliminate the errors from individuals, a pair of mixed samples was used for high-throughput RNA-Seq [Chen et al., 2011]. A total of 61,616 putative lncRNAs were expressed. Up to 166 upregulated and 410 downregulated lncRNAs were expressed with more than twofold change. Moreover, 45 DETs were identified as new transcripts, which had not been functionally characterized. These findings indicate that lncRNAs exhibit a unique expression pattern in AF neural remodeling. Compared with studies on microRNAs, those on lncRNAs are not yet comprehensive. Only few bioinformatic approaches can be used to predict lncRNA functions by interpreting the co-expressed protein-coding genes. GO functional analysis is widely used to illustrate the differentially expressed genes in terms of molecular functions and biological roles. In this study, the main biological processes representing dysregulated lncRNAs were closely associated with neural remodeling, including "positive regulation of developmental process," "cell migration," "neural system development," and "neuron projection regeneration." Similarly, KEGG pathway analysis concluded that the differentially expressed genes mainly belonged to the pathways involved in neural proliferation and neurodegenerative disorders.

Although bioinformatics analysis indicated that the dysregulated genes and the neural remodeling process are strongly coupled, lncRNAs related to ANR can not be selected merely by GO and KEGG pathway analyses. The functions of lncRNAs are also difficult to interpret directly by their nucleotide sequence because little is known about the relationship between the poorly conserved sequence or secondary structure of lncRNAs and their functions [Guo et al., 2013]. Therefore, we adopted a series of filtering steps to identify candidate lncRNAs. First, transcripts with significant expression changes were selected to exclude the potential DETs that may result from the sequencing errors. Besides, it was indicated that lncRNAs could function by modulating the activity and expression of their associated protein-coding genes [Nagano et al., 2008; Rapicavoli et al., 2011]. Moreover, elucidating the biological roles of their target genes would be helpful to decipher the functions of lncRNAs. Thus, lncRNAs with target genes associated with neural remodeling were selected. Bioinformatics analysis of the differentially expressed genes was further performed to confirm their functions. Three candidate lncRNAs were identified. Studies showed that lncRNAs usually exhibit a spatially and temporally restricted expression pattern [Song et al., 2013]. Thus, the transcripts that were highly expressed in skeletal muscles were excluded. Finally, we selected two lncRNAs, namely, TCONS_00032546 and TCONS_00026102, which may play a role in cardiac ANR.

To investigate the potential involvement of the two lncRNAs in AF neural remodeling, loss-of-function experiments were conducted. No significant difference existed for AERP before and immediately after infection between the groups, which suggested that the electrophysiological results were not attributed to the operation of infection. However, after 10 d infection, a significantly shortened AERP was induced by silencing TCONS_00032546, which implied an increased AF vulnerability [Linz et al., 2013]. A significantly elevated nerve density was also observed in the lenti-RNAi-TCONS_00032546 group. Several reports demonstrated that neural regeneration plays a crucial role in promoting the inducibility of AF [Otake et al., 2009], which was consistent with our results. In

summary, these findings indicated that TCONS_00032546 acted as a suppressor in the initiation and maintenance of AF. By the same token, knockdown of the TCONS_00026102 expression decreased nerve density and prolonged AERP, which indicated that TCONS_00026102 positively influenced on AF inducibility.

Although the two lncRNAs exerted important biological effects in AF neural remodeling, the molecular mechanisms by which they modulated these processes remain unknown. Considering that TCONS_00032546 belongs to lincRNAs, accumulating evidence reveals that many lincRNAs may act in cis to regulate the expression of neighboring protein-coding genes because of shared upstream regulations or local transcriptional effects [Ponjavic et al., 2009]. HOTAIR, a classical example of lincRNAs, has been reported to be transcribed from the HOXC locus and regulated the expression of genes from the HOXD locus [Rinn et al., 2007]. HOTTIP, another well-studied *cis*-acting lincRNA, mediates the activation of several 5′ HOXA genes, from which this lincRNA is transcribed [Wang et al., 2011]. Therefore, the mRNA levels of the nearby protein-coding genes were measured to examine whether TCONS_00032546 acted in cis. In contrast to the pacing results, the FGF19 expression increased in the lenti-RNAi-TCONS_00032546 group, which may be ascribed to different situations in comparison. The expression trends of CCND1, FGF4, and FGF3 were also consistent with that of FGF19 after silencing of TCONS_00032546. The CCND1-FGF19-FGF4-FGF3 may act as a gene cluster and is implicated in embryogenesis and carcinogenesis [Salmon et al., 2007]. Although a direct association between the gene cluster and neural outgrowth has not been reported, each molecular in the gene cluster family was closely linked to neurogenesis. Metabotropic glutamate receptors promote the proliferation and differentiation of neural progenitor cells by elevating CCND1 in the brain [Duan et al., 2013]. Wnt7a regulates neural stem cell proliferation by activating the β-catenin-cyclin D1 pathway [Qu et al., 2013]. Further studies indicated that a low concentration of FGF19 can promote chicken statoacoustic ganglion neurite outgrowth and prevent neuronal apoptosis in vitro [Fantetti and Fekete, 2012]. FGF19 also exhibits a neuroprotective effect on adult mammalian photoreceptors in vitro [Siffroi-Fernandez et al., 2008]. Moreover, FGF4 may play a critical role in eliciting the differentiation of astrocytes toward neural progenitor cells [Feng et al., 2014], and KDM7A may regulate neural differentiation through direct transcriptional activation of FGF4, a signal molecule implicated in neural differentiation [Huang et al., 2010]. Several investigations reported that FGF3 is necessary not only for inducing neurogenesis in zebrafish epibranchial placodes [Nechiporuk et al., 2005] but also for promoting the transcriptional activation of genes regulating early specification steps of the zebrafish pituitary cells [Herzog et al., 2004]. Therefore, we hypothesized that the CCND1-FGF19-FGF4-FGF3 gene cluster was a potential target of TCONS_00032546.

Given that TCONS_00026102 is also categorized as a lincRNA, the expression levels of the neighboring protein-coding genes were also examined. Only the expression of SLC25A4 was increased in the lenti-RNAi-TCONS_00026102 group, which was similar to the pacing results. SLC25A4, encoding the ADP/ATP carrier, is highly expressed in heart, skeletal muscle, brain but lowly expressed in proliferating cells [Clémençon et al., 2013]. Similarly, SLC25A4 was associated with neural growth. SLC25A4 mutation is identified in patients with autosomal dominant progressive external ophthalmoplegia [Park et al., 2011]. Plasma membrane-localized adenine nucleotide translocator 1 (also known as SLC25A4) and adenine nucleotide translocator 2 also regulate L1-induced neurite outgrowth of cerebellar neurons in conjunction with matrix metalloprotease 14 [Loers et al., 2012]. Thus, we speculated that SLC25A4 may be a target gene of TCONS_00026102.

Considering that lincRNAs can also function in trans to affect the expression of the genes in different locus, Gene Set Enrichment Analysis was performed to predict the mechanisms of the two lincRNAs in a set of co-expressed mRNAs [Guttman et al., 2009]. Based on the functional terms and literature search, we found that CCND1-FGF19-FGF4-FGF3 gene cluster was associated with the MAPK pathway, whereas SLC25A4 was related to the NF-kappa B pathway. The MAPK pathway is a highly conserved module that is involved in cell proliferation, differentiation and migration. Similarly, each gene in the cluster was coupled with the MAPK pathway in neurogenesis. Metabotropic glutamate receptors play an important role in brain development by increasing CCND1 through activation of ERK1/2 signaling pathways in vitro [Duan et al., 2013]. Tamimi et al. [2006] reported that the forkhead C1 positively regulates FGF19 expression, which is necessary for MAPK phosphorylation in corneal and periocular mesenchymal cells, resulting from neural crest stem cells. FGF4-enhanced neurogenesis of the embryonic stem cells is also related to the activation of JNK-1 and ERK-2 [Chen et al., 2010]. Furthermore, FGF3 is responsible for the patterning of a major transcription factor in the development of the chick hindbrain via activation of the MAPK pathway [Weisinger et al., 2010]. At least three paralleled MAPK pathways are expressed in mammals, including the ERK1/2, JNK, and p38. Therefore, to confirm whether the MAPK pathway was involved in neural remodeling, the expression levels of ERK1/2, JNK, and p38 were assessed in the lenti-RNAi-TCONS_00032546 group. The qRT-PCR results validated the activation of the MAPK pathway. We predicted that TCONS_00032546-mediated neural remodeling may be ascribed to an increased level of CCND1-FGF19-FGF4-FGF3 gene cluster via activation of the MAPK pathway. Although the NF-kappa B pathway, a generic term of a set of transcription factors, regulates genes in immune and inflammatory responses, recent studies demonstrated that recruitment of NF-kappa B participates in the apoptosis-induced overexpression of SLC25A4 [Zamora et al., 2004]. In addition, NF-kappa B pathway plays key regulatory roles in various physiological processes in the nervous system, ranging from neuronal survival to synaptogenesis and plasticity [Crampton and O′Keeffe, 2013]. In the lenti-RNAi-TCONS_00026102 group, the nerve density decreased, which suggested that the apoptotic level increased in the intrinsic cardiac nervous system. Collectively, we inferred that the neuron reduction mediated by TCONS_00026102 was partially attributed to overexpression of SLC25A4 via the NF-kappa B pathway.

Although the two lncRNAs played distinct roles in AF neural remodeling, further studies are needed to illustrate their effects in vitro. Gain-of-function experiments should be conducted to validate the functions of these lncRNAs in subsequent studies. Identification of epigenetic changes, as well as lncRNA–protein and lncRNA–chromatin modifier interactions, would also facilitate understanding of the diverse mechanisms of lncRNAs.

CONCLUSION

This study described the profile of aberrantly expressed lncRNAs in AF and non-AF canine cardiac fat pads by using high-throughput RNA-Seq. These two lncRNAs exerted important biological effects on cardiac ANR during AF, which may be attributed to the regulation of nearby genes. The results suggested a novel functional importance of lncRNAs in AF neural remodeling, thereby providing potential therapeutic targets for prophylaxis and treatment of AF.

ACKNOWLEDGMENTS

A small portion of the manuscript was submitted to the 25th Great Wall International Congress of Cardiology & Asia Pacific Heart Congress and included in the Journal of the American College of Cardiology (JACC) Supplement. (Wang Yuzong; Yinglong Hou. 2014. GW25-e1171 Analysis of long non-coding RNA expression patterns in cardiac fat pads of canine with atrial fibrillation. J Am Coll Cardiol 64 (16_S).).

REFERENCES

Armour JA, Murphy DA, Yuan BX, Macdonald S, Hopkins DA. 1997. Gross and microscopic anatomy of the human intrinsic cardiac nervous system. Anat Rec 247:289–298.

Bu Q, Hu Z, Chen F, Zhu R, Deng Y, Shao X, Li Y, Zhao J, Li H, Zhang B, Lv L, Yan G, Zhao Y, Cen X. 2012. Transcriptome analysis of long non-coding RNAs of the nucleus accumbens in cocaine-conditioned mice. J Neurochem 123:790–799.

Calò L, Rebecchi M, Sciarra L, De Luca L, Fagagnini A, Zuccaro LM, Pitrone P, Dottori S, Porfirio M, de Ruvo E, Lioy E. 2012. Catheter ablation of right atrial ganglionated plexi in patients with vagal paroxysmal atrial fibrillation. Circ Arrhythm Electrophysiol 5:22–31.

Chang CM, Wu TJ, Zhou S, Doshi RN, Lee MH, Ohara T, Fishbein MC, Karagueuzian HS, Chen PS, Chen LS. 2001. Nerve sprouting and sympathetic hyperinnervation in a canine model of atrial fibrillation produced by prolonged right atrial pacing. Circulation 103:22–25.

Chen CW, Liu CS, Chiu IM, Shen SC, Pan HC, Lee KH, Lin SZ, Su HL. 2010. The signals of FGFs on the neurogenesis of embryonic stem cells. J Biomed Sci 17:33.

Chen G, Yin K, Shi L, Fang Y, Qi Y, Li P, Luo J, He B, Liu M, Shi T. 2011. Comparative analysis of human protein-coding and noncoding RNAs between brain and 10 mixed cell lines by RNA-Seq. PLoS ONE 6:e28318.

Clark BS, Blackshaw S. 2014. Long non-coding RNA-dependent transcriptional regulation in neuronal development and disease. Front Genet 5:164.

Clémençon B, Babot M, Trézéguet V. 2013. The mitochondrial ADP/ATP carrier (SLC25 family): Pathological implications of its dysfunction. Mol Aspects Med 34:485–493.

Crampton SJ, O'Keeffe GW. 2013. NF-κB: Emerging roles in hippocampal development and function. Int J Biochem Cell Biol 45:1821–1824.

Duan Z, Zhang X, Zhu GX, Gao Y, Xue X. 2013. Activation of mGluR4 promotes proliferation of rat neural progenitor cells while mediating activation of ERK1/2 signaling pathway. Cell Mol Biol (Noisy-le-grand) 59(Suppl:OL):1809–1817.

Fantetti KN, Fekete DM. 2012. Members of the BMP, Shh, and FGF morphogen families promote chicken statoacoustic ganglion neurite outgrowth and neuron survival in vitro. Dev Neurobiol 72:1213–1228.

Feng GD, He BR, Lu F, Liu LH, Zhang L, Chen B, He ZP, Hao DJ, Yang H. 2014. Fibroblast growth factor 4 is required but not sufficient for the astrocyte dedifferentiation. Mol Neurobiol 50:997–1012.

Guo X, Gao L, Liao Q, Xiao H, Ma X, Yang X, Luo H, Zhao G, Bu D, Jiao F, Shao Q, Chen R, Zhao Y. 2013. Long non-coding RNAs function annotation: A global prediction method based on bi-colored networks. Nucleic Acids Res 41:e35.

Guttman M, Amit I, Garber M, French C, Lin MF, Feldser D, Huarte M, Zuk O, Carey BW, Cassady JP, Cabili MN, Jaenisch R, Mikkelsen TS, Jacks T, Hacohen N, Bernstein BE, Kellis M, Regev A, Rinn JL, Lander ES. 2009. Chromatin signature reveals over a thousand highly conserved large non-coding RNAs in mammals. Nature 458:223–237.

Herzog W, Sonntag C, von der Hardt, Roehl S, Varga HH, Hammerschmidt ZM. 2004. Fgf3 signaling from the ventral diencephalon is required for early specification and subsequent survival of the zebrafish adenohypophysis. Development 131:3681–3692.

Hou Y, Scherlag BJ, Lin J, Zhang Y, Lu Z, Truong K, Patterson E, Lazzara R, Jackman WM, Po SS. 2007. Ganglionated plexi modulate extrinsic cardiac autonomic nerve input: effects on sinus rate, atrioventricular conduction, refractoriness, and inducibility of atrial fibrillation. J Am Coll Cardiol 50:61–68.

Huang C, Xiang Y, Wang Y, Li X, Xu L, Zhu Z, Zhang T, Zhu Q, Zhang K, Jing N, Chen CD. 2010. Dual-specificity histone demethylase KIAA1718 (KDM7A) regulates neural differentiation through FGF4. Cell Res 20:154–165.

Ishii N, Ozaki K, Sato H, Mizuno H, Saito S, Takahashi A, Miyamoto Y, Ikegawa S, Kamatani N, Hori M, Saito S, Nakamura Y, Tanaka T. 2006. Identification of a novel non-coding RNA, MIAT, that confers risk of myocardial infarction. J Hum Genet 51:1087–1099.

Linz D, Mahfoud F, Schotten U, Ukena C, Neuberger HR, Wirth K, Böhm M. 2013. Effects of electrical stimulation of carotid baroreflex and renal denervation on atrial electrophysiology. J Cardiovasc Electrophysiol 24:1028–1033.

Loers G, Makhina T, Bork U, Dörner A, Schachner M, Kleene R. 2012. The interaction between cell adhesion molecule L1, matrix metalloproteinase 14, and adenine nucleotide translocator at the plasma membrane regulates L1-mediated neurite outgrowth of murine cerebellar neurons. J Neurosci 32:3917–3930.

Mercer TR, Dinger ME, Mattick JS. 2009. Long non-coding RNAs: insights into functions. Nat Rev Genet 10:155–159.

Merrick BA, Phadke DP, Auerbach SS, Mav D, Stiegelmeyer SM, Shah RR, Tice RR. 2013. RNA-Seq profiling reveals novel hepatic gene expression pattern in aflatoxin B1 treated rats. PLoS One 8:e 61768.

Nagano T, Mitchell JA, Sanz LA, Pauler FM, Ferguson-Smith AC, Feil R, Fraser P. 2008. The Air noncoding RNA epigenetically silences transcription by targeting G9a to chromatin. Science 322:1717–1720.

Nechiporuk A, Linbo T, Raible DW. 2005. Endoderm-derived Fgf3 is necessary and sufficient for inducing neurogenesis in the epibranchial placodes in zebrafish. Development 132:3717–3730.

Ng J, Villuendas R, Cokic I, Schliamser JE, Gordon D, Koduri H, Benefield B, Simon J, Murthy SN, Lomasney JW, Wasserstrom JA, Goldberger JJ, Aistrup GL, Arora R. 2011. Autonomic remodeling in the left atrium and pulmonary veins in heart failure: Creation of a dynamic substrate for atrial fibrillation. Circ Arrhythm Electrophysiol 4:388–396.

Niland CN, Merry CR, Khalil AM. 2012. Emerging roles for long non-coding RNAs in cancer and neurological disorders. Front Genet 3:25.

Ootsuka S, Asami S, Sasaki T, Yoshida Y, Nemoto N, Shichino H, Chin M, Mugishima H, Suzuki T. 2008. Useful markers for detecting minimal residual disease in cases of neuroblastoma. Biol Pharm Bull 31:1071–1074.

Otake H, Suzuki H, Honda T, Maruyama Y. 2009. Influences of autonomic nervous system on atrial arrhythmogenic substrates and the incidence of atrial fibrillation in diabetic heart. Int Heart J 50:627–641.

Park KP, Kim HS, Kim ES, Park YE, Lee CH, Kim DS. 2011. SLC25A4 and C10ORF2 mutations in autosomal dominant progressive external ophthalmoplegia. J Clin Neurol 7:25–30.

Ponjavic J, Oliver PL, Lunter G, Ponting CP. 2009. Genomic and transcriptional co-localization of protein-coding and long non-coding RNA pairs in the developing brain. PLoS Genet 5:e1000617.

Qu Q, Sun G, Murai K, Ye P, Li W, Asuelime G, Cheung YT, Shi Y. 2013. Wnt7a regulates multiple steps of neurogenesis. Mol Cell Biol 33:2551–2559.

Rapicavoli NA, Poth EM, Zhu H, Blackshaw S. 2011. The long noncoding RNA Six3OS acts in trans to regulate retinal development by modulating Six3 activity. Neural Dev 6:1–15.

Rinn JL, Kertesz M, Wang JK, Squazzo SL, Xu X, Brugmann SA, Goodnough LH, Helms JA, Farnham PJ, Segal E, Chang HY. 2007. Functional demarcation of active and silent chromatin domains in human HOX loci by noncoding RNAs. Cell 129:1311–1323.

Salmon Hillbertz, Isaksson NH, Karlsson M, Hellmén EK, Pielberg E, Savolainen GR, Wade P, von Euler CM, Gustafson H, Hedhammar U, Nilsson A, Lindblad-Toh M, Andersson K, Andersson L. 2007. Duplication of FGF3, FGF4, FGF19 and ORAOV1 causes hair ridge and predisposition to dermoid sinus in Ridgeback dogs. Nat Genet 39:1318–1320.

Shi X, Sun M, Liu H, Yao Y, Song Y. 2013. Long non-coding RNAs: a new frontier in the study of human diseases. Cancer Lett 339:159–166.

Siffroi-Fernandez S, Felder-Schmittbuhl MP, Khanna H, Swaroop A, Hicks D. 2008. FGF19 exhibits neuroprotective effects on adult mammalian photo-receptors in vitro. Invest Ophthalmol Vis Sci 49:1696–1704.

Song G, Shen Y, Zhu J, Liu H, Liu M, Shen YQ, Zhu S, Kong X, Yu Z, Qian L. 2013. Integrated analysis of dysregulated lncRNA expression in fetal cardiac tissues with ventricular septal defect. PLoS ONE 8:e77492.

Spencer SA, Schuh SM, Liu WS, Willard MB. 1992. GAP-43, a protein associated with axon growth, is phosphorylated at three sites in cultured neurons and rat brain. J Biol Chem 267:9059–9064.

Tamimi Y, Skarie JM, Footz T, Berry FB, Link BA, Walter MA. 2006. FGF19 is a target for FOXC1 regulation in ciliary body-derived cells. Hum Mol Genet 15:3229–3240.

Tan AY, Li H, Wachsmann-Hogiu S, Chen LS, Chen PS, Fishbein MC. 2006. Autonomic innervation and segmental muscular disconnections at the human pulmonary vein-atrial junction: Implications for catheter ablation of atrial-pulmonary vein junction. J Am Coll Cardiol 48:132–143.

Trapnell C, Williams BA, Pertea G, Mortazavi A, Kwan G, van Baren MJ, Salzberg SL, Wold BJ, Pachter L. 2010. Transcript assembly and quantification by RNA-Seq reveals unannotated transcripts and isoform switching during cell differentiation. Nat Biotechnol 28:511–515.

Wang KC, Yang YW, Liu B, Sanyal A, Corces-Zimmerman R, Chen Y, Lajoie BR, Protacio A, Flynn RA, Gupta RA, Wysocka J, Lei M, Dekker J, Helms JA, Chang HY. 2011. A long noncoding RNA maintains active chromatin to coordinate homeotic gene expression. Nature 472:120–124.

Wang YZ, Hou YL. 2014. Analysis of long non-coding RNA expression patterns in cardiac fat pads of canine with atrial fibrillation. Asia Pacific Heart Association, conference (Abstract #GW25-e1171).

Weisinger K, Kayam G, Missulawin-Drillman T, Sela-Donenfeld D. 2010. Analysis of expression and function of FGF-MAPK signaling components in the hindbrain reveals acentral role for FGF3 in the regulation of Krox20, mediated by Pea3. Dex Biol 344:881–895.

Wu SC, Kallin EM, Zhang Y. 2010. Role of H3K27 methylation in the regulation of lncRNA expression. Cell Res 20:1109–1116.

Yu B, Zhou S, Hu W, Qian T, Gao R, Ding G, Ding F, Gu X. 2013. Altered long noncoding RNA expressions in dorsal root ganglion after rat sciatic nerve injury. Neurosci Lett 534:117–122.

Zamora M, Meroño C, Viñas O, Mampel T. 2004. Recruitment of NF-kappaB into mitochondria is involved in adenine nucleotide translocase 1 (ANT1)-induced apoptosis. J Biol Chem 279:38415–38423.

Zheng S, Zhang Y, Wang Z, Li Z, Hou X, Duan W, Hou Y. 2014. Autonomic neural remodeling of the pulmonary vein-left atrium junction in a prolonged right atrial pacing canine model. Pacing Clin Electrophysiol 37:745–750.

Zhu JG, Shen YH, Liu HL, Liu M, Shen YQ, Kong XQ, Song GX, Qian LM. 2014. Long noncoding RNAs expression profile of the developing mouse heart. J Cell Biochem 115:910–918.

SUPPORTING INFORMATION

Additional supporting information may be found in the online version of this article at the publisher's web-site.